



On the Use of Fractional-Order Quadrature-Based Moment Closures for Predicting Soot Formation in Laminar Flames

J. Y. Xing, C. P. T. Groth & J. T. C. Hu

To cite this article: J. Y. Xing, C. P. T. Groth & J. T. C. Hu (2022) On the Use of Fractional-Order Quadrature-Based Moment Closures for Predicting Soot Formation in Laminar Flames, Combustion Science and Technology, 194:1, 22-44, DOI: [10.1080/00102202.2019.1678375](https://doi.org/10.1080/00102202.2019.1678375)

To link to this article: <https://doi.org/10.1080/00102202.2019.1678375>



Published online: 17 Oct 2019.



Submit your article to this journal [↗](#)



Article views: 195



View related articles [↗](#)



View Crossmark data [↗](#)



Citing articles: 1 View citing articles [↗](#)

ARTICLE



On the Use of Fractional-Order Quadrature-Based Moment Closures for Predicting Soot Formation in Laminar Flames

J. Y. Xing^a, C. P. T. Groth^a, and J. T. C. Hu^b

^aThe Institute for Aerospace Studies, University of Toronto Institute for Aerospace Studies, Toronto, Ontario, Canada; ^bPratt & Whitney Canada, Mississauga, Ontario, Canada

ABSTRACT

The accurate numerical prediction of soot formation in practical combustion devices remains a challenge. Several new quadrature-based moment closures based on fractional-order moments of soot particle volume are proposed for the prediction of soot formation in laminar diffusion flames at atmospheric and elevated pressures. Both univariate Quadrature Method of Moments (QMOM) models based on a classical particle volume formulation and bivariate Conditional Quadrature Method of Moments (CQMOM) models based on a new particle volume/primary particle number formulation are proposed. The soot models include detailed gas-phase chemistry along with nucleation, surface growth, oxidation, and coalescence/coagulation soot chemistry source terms. Initial comparisons to predictions of a sectional method for space homogeneous simulations illustrate well the improved predictions of soot number density and volume fraction are provided by the fractional-order moment closures compared to integer-order moment approaches. Furthermore, additional comparisons of soot prediction of methane/ethanol laminar diffusion flames at elevated pressures indicate that the proposed bivariate CQMOM, with a specified soot inception size, offer significantly improved results when compared to the other variants and available experimental data.

ARTICLE HISTORY

Received 19 January 2019
Revised 30 September 2019
Accepted 2 October 2019

KEYWORDS

Soot; soot modeling; method of moments; QBMM; CQMOM; CQMOM-Radau; ethanol; laminar diffusion flames

Introduction and motivation

Soot particle formation results from the incomplete combustion of hydrocarbon fuels in various combustion devices such as aircraft gas turbines, diesel engines, and industrial furnaces. Unfortunately, the emission of fine particulate matter can have detrimental effects on both human health and the environment (Pope et al. 2002). Notably, on one hand soot particles are carcinogens and can cause respiratory problems (Kennedy 2007) while on the other hand soot particles contribute to the reduction of arctic ice albedos (Clarke et al. 1967), in addition to possibly induce temperature and precipitation changes (Menon et al. 2002). From this perspective, the accurate prediction of soot formation via numerical modeling is important to designing the next generation of low emission, more environmental friendly, and combustion systems.

Unfortunately, the accurate numerical prediction of soot formation is difficult because of the polydisperse nature of the soot aggregates and the complexity of the chemistry involved.

CONTACT J. Y. Xing  jacques.xing@utias.utoronto.ca  University of Toronto Institute for Aerospace Studies Toronto, Ontario, Canada; C. P. T. Groth  groth@utias.utoronto.ca

Color versions of one or more of the figures in the article can be found online at www.tandfonline.com/gcst.

Notably, the evolution of soot particle size distribution (PSD), which can in many cases be bi- or multi-modal in nature (Zhao et al. 2005), is governed by a high-dimensional integro-differential population balance equation (PBE). Solution techniques of varying complexity and accuracy have been developed to solve this equation in previous studies. For example, stochastic approaches (Balthasar and Kraft 2003; Celnik et al. 2007; Goodson and Kraft 2002; Patterson et al. 2006) represent the soot population by a large number of representative particles, whereas sectional methods (Bhatt and Lindstedt 2009; Blacha et al. 2012; D'Anna and Kent 2006; Smooke et al. 2005; Zhang et al. 2008) involve the solution of transport equations for each of the discrete sections of a discretized size distribution. However, stochastic approaches are generally limited to elementary or academic cases while sectional methods, despite being somewhat less costly, can still be very expensive computationally for practical turbulent flame simulations because of the relatively large number of sections required. Alternatively, the method of moments (Frenklach 2002; Frenklach and Harris 1987; Marchisio et al. 2003; McGraw 1997; Mueller, Blanquart, Pitsch 2009; Salenbauch et al. 2015; Sung et al. 2014; Wick et al. 2017), which requires the solution of only a few transport equations for moments of the distribution function are potentially better suited to practical flame simulations for engineering applications.

The method of moments is gaining in popularity and many different methods have been introduced, such as the Method of Moments with Interpolative Closure (MOMIC) (Frenklach 2002; Frenklach and Harris 1987), the Quadrature Method of Moments (QMOM) (Marchisio et al. 2003; McGraw 1997), the Extended Quadrature Method of Moments (EQMOM) (Chalons, Fox, Massot 2010; Madadi-Kandjani and Passalacqua 2015; Yuan, Laurent, Fox 2012), and the Conditional Method of Moments (CQMOM) (Buffo, Vanni, Marchisio 2012; Yuan and Fox 2011). While several of these moment methods have been used for soot prediction (Frenklach 2002; Frenklach and Harris 1987; Salenbauch et al. 2015; Wick et al. 2017; Zucca et al. 2006), comparisons of the predictive capabilities of the various moment techniques to each other and other methods is lacking. Furthermore, the relative importance of fractional-order moments (McGraw and Wright 2003; Wright, McGraw, Rosner 2001) has not been considered for soot prediction.

A first goal of the current study is therefore to validate and compare the accuracy of various Quadrature-Based Method of Moments (QBMM) methods, including QMOM, QMOM-Radau, EQMOM, CQMOM, and CQMOM-Radau methods, to a sectional method for space-homogeneous problems for both integer-order and fractional-order moments. The resulting fractional-order quadrature-based moments methods are subsequently applied to the prediction of soot formation in a laminar diffusion flames and their predictions compared to the by now almost standard two-equation semi-empirical model for soot transport and formation (Leung, Lindstedt, Jones 1991; Liu et al. 2002). The discussion includes theoretical descriptions of the various moment closures considered along with comparisons of the predictions of soot formation in methane/ethanol laminar diffusion flames at elevated pressures. The latter are obtained by making use of the computational framework for the prediction of soot formation in laminar flames originally developed by Charest, Groth, Gülder (2010).

Soot aerosol modeling

As mentioned in the introduction, the evolution of the soot particle density number, $n(\vec{x}; \vec{\epsilon})$, is governed by a PBE given by

$$\begin{aligned} \frac{\partial n(\vec{x}; \vec{\varepsilon})}{\partial t} + \frac{\partial}{\partial x_j} \left((u_j + V_{T_j}) n(\vec{x}; \vec{\varepsilon}) \right) - \frac{\partial}{\partial x_j} \left(D_s \frac{\partial n(\vec{x}; \vec{\varepsilon})}{\partial x_j} \right) \\ = \frac{dn(\vec{x}; \vec{\varepsilon})}{dt} \Big|_{nuc+agg+sg+cond+ox} \end{aligned} \quad (1)$$

where $\vec{\varepsilon}$ are parameters (e.g. particle volume, V) characterizing the soot particles, u_j is the flow velocity, D_s is the soot diffusion coefficient, and V_T is the thermophoretic velocity of the particles. The right-hand side of Eq. (1) represents various source terms which notably include the effects of nucleation (nuc), agglomeration (agg), surface growth (sg), condensation (cond), and oxidation (ox). A brief review of common solution techniques for this PBE, including section and moment closure methods, will now be described in what follows below.

Sectional method

In this study, a univariate volume-based ($\vec{\varepsilon} = V$) sectional method is used to provide reference numerical solutions to the balance equation of Eq. (1) for space homogeneous problems. In the univariate case, the soot particles are assumed to be spherical in shape with $V = 4\pi r^3/3$ where r is the particle radius. For the sectional method implemented in this study, a fixed discrete sectional method is used to discretize the soot PSD function and thereby allowing the description of polydisperse spherical aerosol. Each section, i , has a fixed representative volume, V_i , with a specified spacing factor, f_s , such that

$$V_{i+1} = f_s V_i, \quad (2)$$

with $i = 1, 2, \dots, N_s$, where N_s is the number of sections. Typically, N_s must be large (i.e., $N_s > 100$) to ensure high accuracy and, even for more practical simulations, values of $N_s = 20-40$ are still required to ensure reasonable accuracy for engineering accuracy (Bhatt and Lindstedt 2009; Blacha et al. 2012; D'Anna and Kent 2006; Smooke et al. 2005; Zhang et al. 2008).

The fixed boundary between any two sections, i and $i + 1$, is given by

$$V_{b,i} = \frac{1}{2} (V_i + V_{i+1}). \quad (3)$$

A discrete total density number, N_i , is assigned to each section volume, V_i , resulting in a piecewise Dirac representation of the distribution function. The average density number per section is then given by

$$n_i = \frac{N_i}{V_{b,i+1} - V_{b,i}}. \quad (4)$$

The various component of the source term of the discrete density number for each section, i , can be treated individually and expressed as

$$\frac{dN_i}{dt} \Big|_{nuc+agg+sg+cond+ox} = \frac{dN_i}{dt} \Big|_{nuc} + \frac{dN_i}{dt} \Big|_{agg} + \frac{dN_i}{dt} \Big|_{sg} + \frac{dN_i}{dt} \Big|_{cond} + \frac{dN_i}{dt} \Big|_{ox}. \quad (5)$$

The evaluation of each of these source terms is discussed in more detail below.

Nucleation

The soot particles are assumed here to nucleate at a single inception size, V_0 , such that

$$\left. \frac{dN_1}{dt} \right|_{nuc} = \dot{r}_{nuc}, \quad (6)$$

where \dot{r}_{nuc} is the prescribed rate of nucleation.

Coagulation

Coagulation is treated in this study with the fixed pivot technique (FPT) of Kumar and Ramkrishna (Kumar and Ramkrishna 1996) that allows the conservation of both total density number and total mass (or volume) with

$$\left. \frac{dN_i}{dt} \right|_{agg} = \sum_{\substack{k \leq j \leq i \\ m_{i-1} \leq V_j + V_k \leq V_{i+1}}} \left(1 - \frac{\delta_{j,k}}{2} \right) \eta \beta_{j,k} N_j N_k - N_i \sum_{k=1}^M \beta_{i,k} N_k \quad (7)$$

where $\delta_{j,k}$ is the Kronecker delta tensor and $\beta_{i,k}$ (or $\beta_{j,k}$) is the agglomeration frequency. The parameter, η , is introduced in order to conserve both total density number and total volume, and is given by the expression

$$\eta = \begin{cases} \frac{V_{i+1} - (V_j + V_k)}{V_{i+1} + V_i}, & V_i \leq V_j + V_k \leq V_{i+1} \\ \frac{V_{i-1} - (V_j + V_k)}{V_{i-1} + V_i}, & V_{i-1} \leq V_j + V_k \leq V_i. \end{cases} \quad (8)$$

Surface growth, condensation, oxidation

Soot surface growth, condensation, and oxidation are treated herein with a second-order finite-volume method (FVM) (Qamar et al. 2006) adapted to a discrete formulation. For surface growth, the source term can be written as

$$\begin{aligned} \left. \frac{dN_i}{dt} \right|_{sg} = & -\dot{r}_{sg} \left(\frac{S_i + S_{i+1}}{2} \right) [n_i + 0.5\phi_i(n_i - n_{i-1})] \\ & + \dot{r}_{sg} \left(\frac{S_{i-1} + S_i}{2} \right) [n_{i-1} + 0.5\phi_{i-1}(n_{i-1} - n_{i-2})] \end{aligned} \quad (9)$$

where \dot{r}_{sg} is the specific surface growth rate and S_i is the sectional surface area. The slope limiter function, ϕ_i , given by

$$\phi_i = \max \left\{ 0, \min \left[2q_i, \min \left(\frac{1}{3} + \frac{2}{3}q_i, 2 \right) \right] \right\}, \quad (10)$$

is used for computational robustness with

$$q_i = \frac{n_{i+1} - n_i + \epsilon}{n_i - n_{i-1} + \epsilon}, \quad (11)$$

where ϵ is a small value (10^{-12}) used to avoid division by 0. Condensation and oxidation are treated in similar fashions.

QMOM/QMOM-Radau closure

Various quadrature-based moment closure techniques are now considered. In QMOM (Marchisio et al. 2003; McGraw 1997) closures, rather than solving directly the PBE for $n(\vec{\epsilon})$, the distribution function is represented as a sum of Dirac delta functions with quadrature weight and point (volume abscissa) such that closure of the source terms can then be achieved by direct numerical quadrature. For a univariate description with $\vec{\epsilon} = V$, the soot is represented as a polydisperse aerosol of spherical particles and the corresponding approximate distribution is defined by

$$n(V) = \sum_{i=1}^{N_V} N_i \delta(V - V_i), \quad (12)$$

and the k^{th} -order volume moment is then given by

$$M_k = \sum_{i=1}^{N_V} N_i V_i^k, \quad (13)$$

where N_V is the number of volume Dirac function, N_i are the weights, and V_i are the volume abscissa. The weights and abscissa of the Dirac functions defining the approximated distribution for soot particle size can be evaluated directly from a set of $2N_V$ known moments via a moment-inversion algorithm such as the Product-Difference (PD) (Gordon 1968) or Wheeler (Wheeler 1974) algorithms. The main idea in such solution approaches is to use orthogonal polynomials to construct a Jacobi matrix of the form

$$\mathbf{J} = \begin{bmatrix} a_0 & \sqrt{b_1} & & & & \\ \sqrt{b_1} & a_1 & \sqrt{b_2} & & & \\ & \sqrt{b_2} & \ddots & \ddots & & \\ & & \ddots & \ddots & \ddots & \\ & & & \sqrt{b_{N_V-1}} & & \\ & & & \sqrt{b_{N_V-1}} & a_{N_V-1} & \end{bmatrix}. \quad (14)$$

The abscissa, V_i , and weights, N_i , are then given respectively by the eigenvalues and eigenvectors of the preceding Jacobi matrix, \mathbf{J} .

The PD and Wheeler moment inversion algorithms require integer-order moments; however, QMOM methods can be generalized to fractional-order moments by introducing a variable change such that the moments are alternatively defined by

$$M_k = M_{x/k_s} = \sum_{i=1}^{N_V} N_i V_i^{x/k_s} = \sum_{i=1}^{N_V} N_i \tilde{V}_i^x, \quad (15)$$

where x are the corresponding integer moments orders, k are the fractional moments orders, and k_s is the fraction denominator. The general formulation of Eq. (15) reduces to integer-

order formulation when $k_s=1$. Typically, the number of quadrature points, N_V , is chosen to $N_V = 2-6$ for space homogeneous problems and $N_V = 2-3$ for multidimensional flow problems. The influence of N_V will be explored for space homogeneous problems in this study. A variation of the QMOM method, with one fixed quadrature at the inception size V_0 , is known as a QMOM-Radau method (Salenbauch et al. 2015) and is also considered here. The number of moments to be solved in this case is then equal to $2N_V - 1$. In this study, implementations of both QMOM and QMOM-Radau univariate closures are considered which account for nucleation, surface growth, oxidation, and agglomeration.

EQMOM closure

Rather than representing the distribution function as a sum of Dirac delta functions, an alternative approximate approach is to make use of presumed kernel functions for the density distribution of the soot particles. This so-called EQMOM approach was first introduced by Chalons, Fox, Massot (2010) where Gaussian kernel functions were used. Yuan, Laurent, Fox (2012) have further developed the EQMOM approach for both gamma and beta kernel functions while Madadi-Kandjani and Passalacqua (Madadi-Kandjani and Passalacqua 2015) extended the method for log-normal distributions. In the EQMOM approach, the distribution function for a monovariate case, $n(\vec{\epsilon} = V)$, is therefore given by

$$n(V) = \sum_{i=1}^{N_{\mathcal{F}}} N_i \mathcal{F}(V; \chi_i, \sigma), \quad (16)$$

where $N_{\mathcal{F}}$ is the total number of kernel functions (typically, $N_{\mathcal{F}} = 2-5$) and $\mathcal{F}(V; \chi_i, \sigma)$ is the assumed shape of kernel functions. The weights, N_i , the size parameter, χ_i , and the shape parameter, σ , of the kernel functions are computed from $2N_{\mathcal{F}} + 1$ known (computed) moments. The source terms are then closed from the resulting distribution function by a secondary quadrature procedure. In order to continue to exploit the PD or Wheeler algorithm for the solution of the moment inversion problem in a EQMOM approach, a transformation is again required.

In this study, log-normal kernel functions, of the form

$$\mathcal{L}(V; \chi_i, \sigma) = \frac{1}{V\sigma\sqrt{2\pi}} \exp\left(-\frac{(\ln(V) - \chi_i)^2}{2\sigma^2}\right), \quad (17)$$

are used. The log-normal distribution is defined on the interval $[0, 908[$ and in order to avoid particle distribution of zero size, the log-normal distributions are shifted by the value of V_0 as in (Salenbauch et al. 2015). The resulting $2N_{\mathcal{F}} + 1$ moments are given by

$$\tilde{M}_k = \sum_{r=0}^k \binom{k}{r} M_{k-r}(-V_0)^r, \quad (18)$$

where

$$\tilde{M}_k = \sum_{i=1}^{N_{\mathcal{F}}} N_i V_i^k \exp\left(\frac{k^2 \sigma^2}{2}\right), \quad (19)$$

with $V_i = \exp(\chi_i)$. The transformed moments, M_k^* , are then given by

$$M_k^* = \frac{\tilde{M}_k}{\exp(k^2 \sigma^2 / 2)} = \sum_{i=1}^{N_{\mathcal{F}}} N_i V_i^k, \quad (20)$$

where the shape parameter, σ , is computed iteratively through a root-finding approach. Because of the binomial theorem used for the moment translation, fractional-order moments have not been considered herein for the log-normal EQMOM approach. Nevertheless, the current implementation of the EQMOM closures account for nucleation, surface growth, oxidation, and agglomeration.

CQMOM/CQMOM-Radau closure

A multivariate moment closure description allows for a more realistic representation of soot aerosols as polydisperse aggregates instead of treating the soot as a simple collection of spherical particles. The fractal-like aggregate nature of soot particulate matter arising from combustion processes, consisting of linked chain-like structures of primary particles, has been well established experimentally (Köylü et al. 1995). While volume and surface area have been previously suggested to define the related macroscopic moments of soot aggregates (Mueller, Blanquart, Pitsch 2009; Salenbauch et al. 2015; Sung et al. 2014), the current study proposes the use of the volume, V , representing the size of the primary particles in the aggregates and the number of primary particles, n_p , making up the soot aggregates (the latter are assumed to consist of multiple primary particles). As such, the current multivariate description uses $\vec{\epsilon} = [V, n_p]$. It should be noted that, although primary particle number was used as secondary variable by Frenklach (Frenklach 2002), the pseudo-bivariate MOMIC method described therein can only treat pure moments. Conversely, the proposed multivariate QMOM approaches allow for the description of mixed moments and can better represent the complex nature of soot particles. Nevertheless, direct inversion of the moments to recover the corresponding weights and abscissa can be difficult in multivariate QMOM methods. The moment inversion problem for the multivariate case can however be simplified by applying a so-called CQMOM closure approach (Buffo, Vanni, Marchisio 2012; Yuan and Fox 2011), which represents the multivariate density distribution as a product of conditional density functions.

The form of the approximate distribution function in the proposed bivariate CQMOM and CQMOM-Radau closure is then given by

$$\begin{aligned} n(V, n_p) &= \sum_{i=1}^{N_V} \sum_{j=1}^{N_{n_p}} N_{ij} \delta(V - V_i) \delta(n_p - n_{p_{ij}}) \\ &= \sum_{i=1}^{N_V} \sum_{j=1}^{N_{n_p}} w_i w_{ij} \delta(V - V_i) \delta(n_p - n_{p_{ij}}), \end{aligned} \quad (21)$$

while the corresponding known moments sets, $M_{k,\ell}$, are defined by

$$M_{k,\ell} = \sum_{i=1}^{N_V} \sum_{j=1}^{N_{np}} N_{ij} V_i^k n_{p_{ij}}^\ell = \sum_{i=1}^{N_V} \sum_{j=1}^{N_{np}} w_i w_{ij} V_i^k n_{p_{ij}}^\ell, \quad (22)$$

where N_V is the number of Dirac functions for primary particle volume and N_{np} is the number of Dirac functions for primary particle number. The total number of Dirac functions, N_D , is then $N_V N_{np}$, with typically $N_V = 2-3$ and $N_{np} = 1-2$ for multidimensional flow problems. Also, N_{ij} represents the quadrature density number, w_i are the volume quadrature weight, w_{ij} are the conditional primary particle quadrature weight, V_i are the primary particle volume abscissa, and $n_{p_{ij}}$ are the conditional primary particle number. A total of $2N_V + N_V(2N_{np} - 1)$ known moments are then considered with $2N_V$ pure moments defined in a QMOM closure using

$$M_{k,0} = \sum_i^{N_V} w_i V_i^k \quad (23)$$

This allows one to find the volume nodes, V_i , and volume weights, w_i . The conditional primary particle node information can then be determined from

$$M_{k,\ell} = \sum_{i=1}^{N_V} \sum_{j=1}^{N_{np}} w_i w_{ij} V_i^k n_{p_{ij}}^\ell = \sum_{i=1}^{N_V} w_i V_i^k \tilde{N}_{p_{i,\ell}}. \quad (24)$$

By solving the system given by Eq. (24), the values of $\tilde{N}_{p_{i,\ell}}$ can be computed by using

$$\begin{bmatrix} M_{0,\ell} \\ M_{1,\ell} \\ \vdots \\ M_{N_V-1,\ell} \end{bmatrix} = \begin{bmatrix} 1 & 1 & \dots & 1 \\ V_1 & V_2 & \dots & \\ \vdots & \vdots & \ddots & \vdots \\ V_1^{N_V-1} & V_2^{N_V-1} & \dots & V_{N_V}^{N_V-1} \end{bmatrix} \begin{bmatrix} w_1 \\ w_2 \\ \vdots \\ w_{N_V} \end{bmatrix} \begin{bmatrix} \tilde{N}_{p_{1,\ell}} \\ \tilde{N}_{p_{2,\ell}} \\ \vdots \\ \tilde{N}_{p_{N_V,\ell}} \end{bmatrix} \quad (25)$$

with $\tilde{N}_{p_{i,0}} = 1$. Once the values of $\tilde{N}_{p_{i,\ell}}$ are known, it is possible to use the PD or Wheeler algorithm for each volume node to evaluate the value of w_{ij} and $n_{p_{ij}}$ using the relation

$$\tilde{N}_{p_{i,\ell}} = \sum_{j=1}^{N_{np}} w_{ij} n_{p_{ij}}^\ell. \quad (26)$$

As with the QMOM approach, the CQMOM moment closures can be extended to fractional-order moments by introducing a variable change and expressing the moments of interest as

$$M_{k,\ell} = M_{x/k_s, y/\ell_s} = \sum_{i=1}^{N_V} \sum_{j=1}^{N_{np}} N_{ij} V_i^{x/k_s} n_{p_{ij}}^{y/\ell_s} = \sum_{i=1}^{N_V} \sum_{j=1}^{N_{np}} N_{ij} \tilde{V}_i^x \tilde{n}_{p_{ij}}^y, \quad (27)$$

where x and y are integer-order moments, k and ℓ are fractional-order moments, k_s and ℓ_s are the fraction denominators. Again, the general formulation of Eq. (27) reduces to integer-order formulation when $k_s = 1$ and $\ell_s = 1$. Also similar to the QMOM-Radau closures described previously, it is possible to fix one volume quadrature point at the inception size, V_0 . Such a variant is also considered here and will be referred to as CQMOM-Radau closure. The number of moments to be considered in the closure is then reduced and is equal to $2N_V - 1 + (N_V - 1)(2N_{np} - 1)$ in this case. As with the other moment closures considered here, all of the CQMOM/CQMOM-Radau method implementations of this study consider the effects of nucleation, surface growth, oxidation, and aggregation.

Numerical results and discussion

Numerical results obtained with both the integer- and fractional-order QBMMs proposed here are first validated for a space-homogeneous problem and their predictive capabilities are compared to those of the present sectional method. The proposed fractional-order moment QBMMs are subsequently applied to the prediction of soot formation in methane/ethanol laminar diffusion flames at elevated pressures, for which the numerical predictions are compared to available experimental data (Griffin, Christensen, Gülder 2018), as well as to the predictions of standard two-equation empirical models for soot formation.

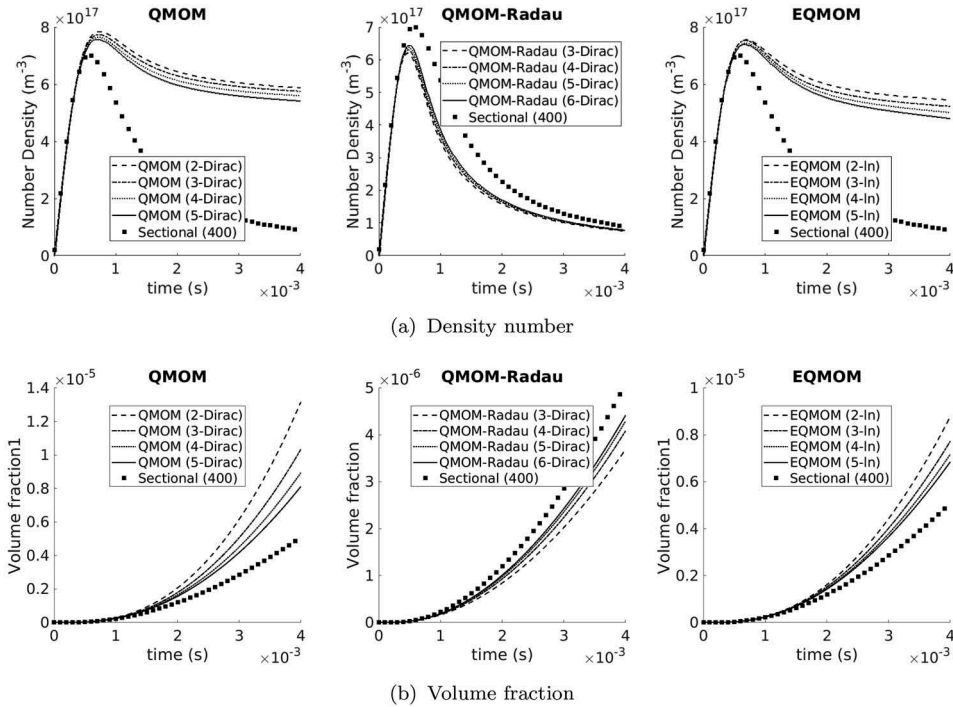
Space-homogeneous problem

Numerical solutions of a space-homogeneous aerosol problem that includes the effects of nucleation, agglomeration, and surface growth were determined numerically for the univariate QMOM, EQMOM, and QMOM-Radau with integer-order moments and for the univariate QMOM and QMOM-Radau with fractional-order moments. The parameters used for the evaluation of the various source terms are indicated in Table 1. The QBMM results are compared to those obtained using the univariate sectional method with $N_s = 400$ sections and a spacing factor of 1.045. Since no analytical solution exist for this example case, the sectional method results with a high value for N_s serve as a reference solution for comparison of the various quadrature-based moment closures.

The computed evolution of the density number and volume fraction with time for $t = 0-4$ ms are shown in Figures 1 and 2 for integer-order moments and fractional-order moments, respectively. The number of moments considered ranged from 4 to 12 for QMOM and 5 to 11 for EQMOM and QMOM-Radau. For the fractional-order moments, $k_s = 3$ was used, which basically converts the volume-based formulation into a diameter-based formulation. In comparing the moment closure and sectional method results, Figure 1 indicates that significant improvements in the prediction of the evolution of the density number are achieved by the QMOM-Radau methods relative to the QMOM approaches for integer-order moments, while only marginal improvement is observed with EQMOM methods. Additionally, Figure 2 indicates that the evolution of density number and volume fraction are both predicted much more accurately with fractional-order moments for both QMOM and QMOM-Radau, with the differences between the two being rather small.

Table 1. Soot chemistry parameters for the space-homogeneous case.

Nucleation	$r_{nuc} = 20 \cdot 10^{20} s^{-1}$ $V_0 = 500 \cdot 10^{-30} m^3$
Surface growth	$r_{sg} = 2000 \cdot 10^{20} m^{-2} s^{-1}$ $dV_{sg} = 25 \cdot 10^{-30} m^3$
Coagulation	Harmonic mean collision kernel with $\eta = 1.0$ $T = 1800 \text{ K}$ $P = 101,325 \text{ Pa}$


Figure 1. Prediction of the evolution of the (a) density number (b) and volume fraction with integer order moment QBMM for the space-homogenous problem.

Convergence of the final density number and volume fraction at the maximum time of $t = 4 \text{ ms}$ with number of moments are shown in [Figure 3](#). The results indicate that rather slow convergence is observed with the number of integer-order moment for the prediction of the density number while the convergence is significantly improved with increasing fractional-order moments. This is explained by the fact that with higher-order moments, the Dirac quadrature distribution is biased toward the tail of the distribution. Hence, with integer-order moment, QMOM-RADAU methods show significant improvement relative to the QMOM closures as they explicitly assign one quadrature node to the inception size while, for fractional-order moments, the improvement due to an additional quadrature at the inception size is somewhat more limited. This is confirmed by the additional results in [Figures 4](#) and [5](#). The sectional method results predict a bimodal distribution with a inception mode that is not captured

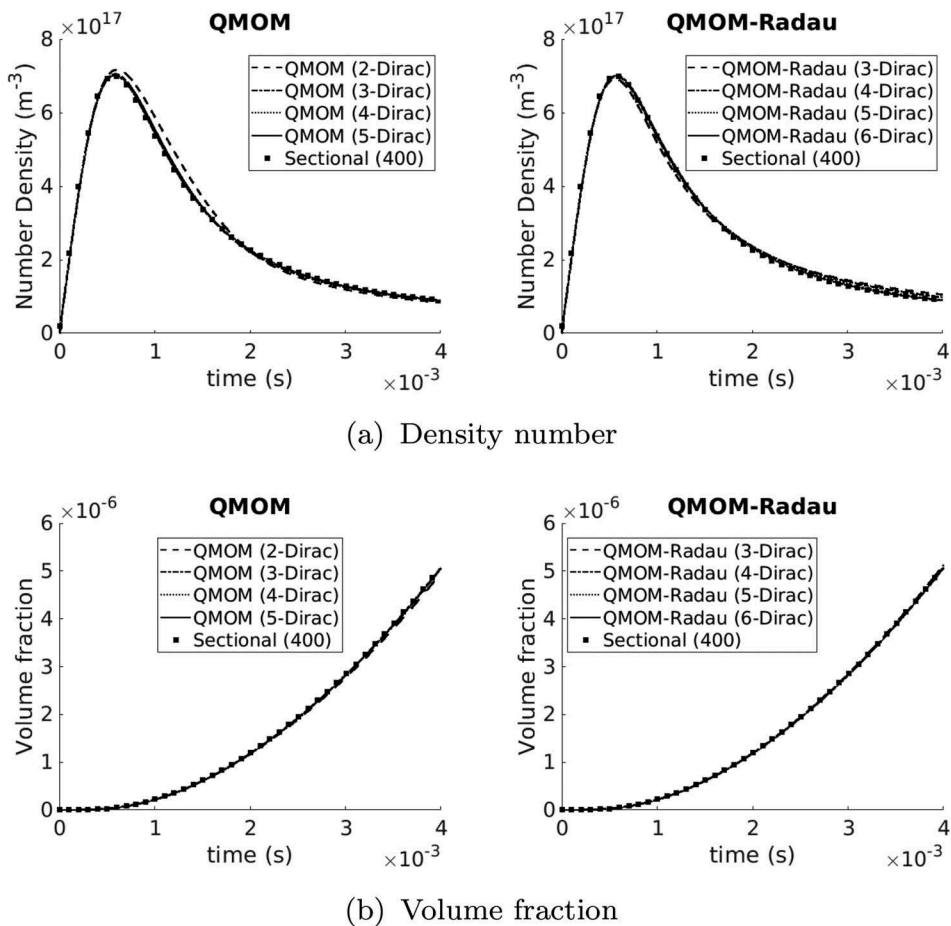


Figure 2. Prediction of the evolution of the (a) density number (b) and volume fraction with fractional order moment QBMM for the space-homogenous problem.

appropriately by any node of the integer-order moments QMOM approaches, while the fractional-order moment QMOM approaches result in some portion of the quadrature points in the vicinity of the inception size, which lead to improved solution quality. The importance of the inception mode for soot modeling is explained by the large range of size covered by soot particles from incipient particle of about 10^{-27}m^3 to large aggregate of about 10^{-20}m^3 which corresponds to a volume-equivalent diameter of a few hundreds of nm. Hence, with an integer-order moment formulation, the contribution of the quadrature points representing the small particle size is eclipsed by numerical rounding errors in the determination of higher-order moments. Consequently, adding more quadrature points in an integer-order moment formulation does not significantly improve the quality of the predictions for cases with a bimodal distribution. Application of fractional-order moments for soot modeling is thus of significant importance, particularly as experiments (Zhao et al. 2005) indicate that soot particle distribution can have a bimodal structure.

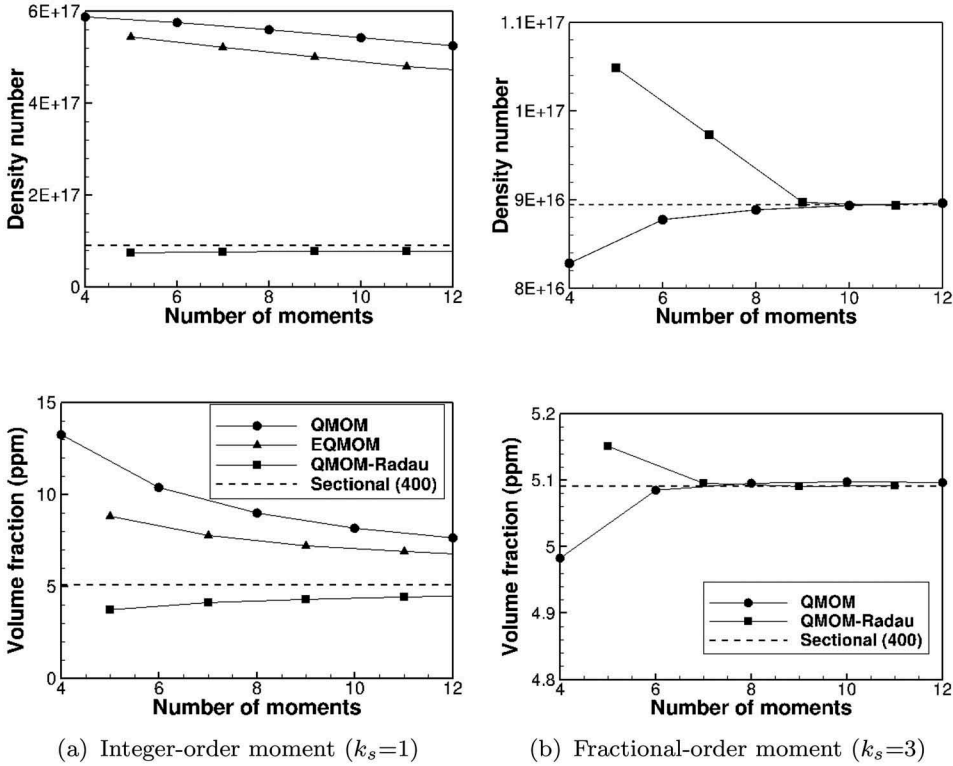


Figure 3. Convergence of the QBMM moment closures with (a) integer-order and (b) fractional-order moments for the space-homogenous problem at time $t = 4$ ms.

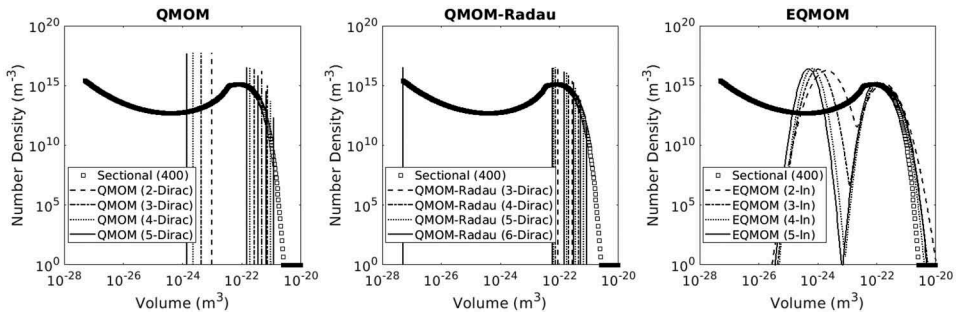


Figure 4. Size distributions for QBMMs with integer-order moment ($k_s = 1$) for the space-homogeneous case at time $t = 4$ ms.

UTIAS high-pressure laminar coflow burner

Charest, Groth, Gülder (2010) previously developed a computational framework for the prediction of soot formation in laminar diffusion flames. In this framework, the Navier-Stokes equations for laminar flows of a multicomponent gas with complex chemistry are discretized by a FVM using a second-order piecewise limited reconstruction for the

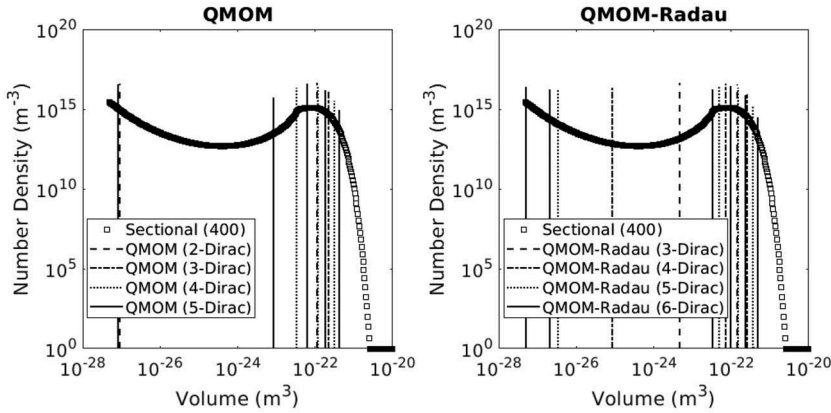


Figure 5. Size distributions for QBMMs with fractional-order moment ($k_s=3$) for the space-homogeneous case at time $t=4$ ms.

evaluation of inviscid fluxes while a diamond path is used for the evaluation of the viscous fluxes. Low-Mach preconditioning is introduced in order to reduce excessive numerical dissipation and numerical stiffness. Steady-state solutions of the discrete solutions are obtained by an inexact Newton-Krylov-Schwarz (NKS) algorithm while radiative heat transfer is solved with discrete-ordinate-method (DOM) for a non-gray media. The computational framework of Charest, Groth, Gülder (2010) has been previously used to predict soot formation in elevated pressure laminar diffusion flames for a variety of fuels ranging from ethylene (Charest et al. 2011), methane (Charest, Groth, Gülder 2011), and biogas (Charest, Gülder, Groth 2014). For this study, the original soot prediction capabilities (two-equation empirical soot model) have been expanded to include the proposed fractional-order QBMM models for $N_V=3$ and $N_{n_p}=1$. Note that the results of the numerical study for the space-homogeneous problem described previously indicate that this number of quadrature points offers a good compromise between computational cost and numerical accuracy. The corresponding sets of macroscopic moments considered in the various closures are indicated in Table 2.

For the current study, the UTIAS elevated-pressure methane-ethanol laminar coflow burner with a 10% carbon mass from ethanol (Griffin, Christensen, Gülder 2018) is considered to validate the proposed quadrature based moment closures for soot. The burner configuration and experimental conditions used for the simulations are indicated in Table 3. The computational domain is divided into 506 blocks with a total of 60,720 computational cells. Schematic views of the burner, along with the computational mesh used herein, are shown in Figure 6. A reduced Dryer mechanism (29 Species, 154 reactions) (Akih-Kumgeh 2013) is used in this study to model the complex gas-phase chemistry.

For the simulations performed herein, the soot source terms associated with the moment closures were evaluated using an explicit time-discretization and a splitting approach (Sung et al. 2014) in order to preserve moment realizability. Nucleation was modeled by using a simplified acetylene-based precursor model (Liu et al. 2002), while surface growth was modeled by using the HACA mechanism of Blanquart and Pitsch (Blanquart and Pitsch 2009). Oxidation of the soot particulates by O_2 was modeled from

Table 2. Soot moment set for QMOM, QMOM-Radau, CQMOM, CQMOM-Radau with $N_V = 3$ and $N_{n_p} = 1$.

QMOM	$M_0, M_{1/3}, M_{2/3}, M_1, M_{4/3}, M_{5/3}$
QMOM-Radau	$M_0, M_{1/3}, M_{2/3}, M_1, M_{4/3}$
CQMOM	$M_{0/3,0}, M_{1/3,0}, M_{2/3,0}, M_{1,0}, M_{4/3,0}, M_{5/3,0}, M_{0,1}, M_{1/3,1}, M_{2/3,1}$
CQMOM-Radau	$M_{0/3,0}, M_{1/3,0}, M_{2/3,0}, M_{1,0}, M_{4/3,0}, M_{0,1}, M_{1/3,1}$

Table 3. UTIAS elevated-pressure burner configuration and experimental conditions.

Inlet length	5.0 mm
Fuel tube diameter	3.06 mm
Coflow diameter	25.4 mm
Fuel mass flow	1.221 mg/s
Air mass flow	0.340 g/s
Fuel temperature	473 K
Air temperature	473 K
Pressure	1, 2, 4, and 6 atm
Fuel	$\text{CH}_4/\text{C}_2\text{H}_5\text{OH}$

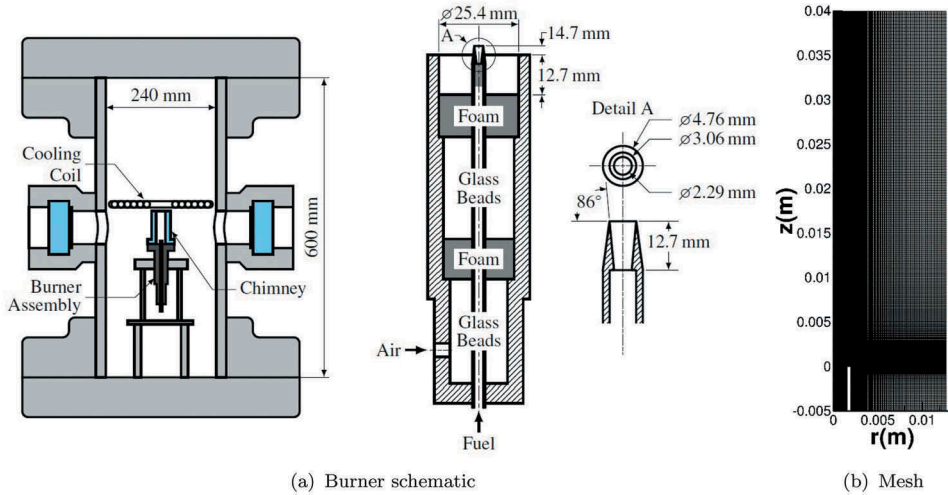


Figure 6. UTIAS high-pressure burner showing: (a) schematic view and (b) computational mesh.

the reaction rate of the ABF model (Appel, Bockhorn, Frenklach 2000), while a collision efficiency of 0.10 was assumed for oxidation by O and OH. The proposed soot chemistry model used here is summarized in Table 4. The predicted numerical results for the various laminar flames are compared to both the available experimental results as well as to results

Table 4. Soot chemistry parameters.

Nucleation	Liu et al. (Liu et al. 2002)
Surface growth	Blanquart and Pitsch (Blanquart and Pitsch 2009)
Oxidation (O_2)	ABF (Appel, Bockhorn, Frenklach 2000)
Oxidation (O)	$\eta_{\text{O}} = 0.10$
Oxidation (OH)	$\eta_{\text{OH}} = 0.10$
Coagulation	Harmonic mean collision kernel with $\eta = 0.20$

obtained using the original two-equation soot model used in the framework of Charest *et al.* with both the proposed chemistry submodel and the two-equation model previously proposed by Liu *et al.* (2002), respectively. The latter notably artificially neglects soot coagulation in order to predict the evolution of the primary particles.

The predicted temperature and soot distributions obtained with the various soot models are shown in Figures 7 and 8, respectively, for pressures of 2, 4, and 6 atm. It is evident that the predicted flame structure is not strongly affected by the differences between the soot models, except for the two-equation model with the chemistry submodel of Liu *et al.*, which exhibits a temperature difference of 10–20 K from the other results. This temperature difference is explained by the higher soot volume fraction predicted by the latter. Comparison of peak soot concentrations with experimental data (Griffin, Christensen, Gülder 2018) are indicated in Table 5. The tabulated results indicate only minor differences between QMOM and QMOM-Radau and between CQMOM and CQMOM-Radau moment closures. Hence, by fixing one quadrature point at the inception size it is possible to achieve identical predictions using just a few macroscopic moments. In addition, the results indicate that the two-equation model of Liu *et al.*, which was calibrated for ethylene flames, overestimates the peak soot concentration for this burner configuration at all pressures. On the other hand, the results further indicate that the QMOM/QMOM-Radau moment closures under predict the peak soot concentration in the diffusion flames as all of these univariate descriptions only consider pure coalescence, which results in a underestimation of soot surface area. Table 5 also indicates that the two-equation model with the current chemistry submodel provides better prediction of the peak soot concentration for all pressures considered when compared to the univariate QMOM/QMOM-Radau closures. This apparently surprising result is explained by the fact that the monodisperse description of the two-equation model artificially overestimates the soot surface area for a given soot volume fraction and density number. Finally, the bivariate CQMOM/CQMOM-Radau moment closures provide better predictions of the peak soot formation than the QMOM/QMOM-Radau approaches, as they consider soot aggregation which provides a more correct estimation of soot surface area.

The predicted radial profiles of the soot volume fraction are also given in Figures 9–11 for the laminar flames of interest at pressures of 2, 4, and 6 atm. The two-equation model with the chemistry submodel of Liu *et al.* calibrated to predict peak soot concentration of atmospheric pressure ethylene flames, systematically overpredicts soot volume fraction at all pressures and axial locations, but seems to better predict the centerline soot concentrations than the other methods. However, this is more likely due to an artifact from the overprediction of soot peak concentrations. Moreover, the two-equation model of Liu *et al.*, does not predict well the variations in the soot radial profiles. These findings highlight some of the limitations of semi-empirical two-equation models when applied to different flames other than those used in their original calibration. On the other hand, all of the soot models with the proposed chemistry submodel, including the two-equation model, predict relatively well the shape of soot volume fraction distributions except at the centerline. The significant underprediction of soot formation near the centerline for all of the models can be explained by the simplified non-PAH-based acetylene mechanism used as the soot precursor. The current comparisons of the radials profiles however also clearly illustrate the superior performance of the CQMOM-Radau moment closure over the other approaches in predicting the radial distributions of soot volume fraction for the cases considered here.

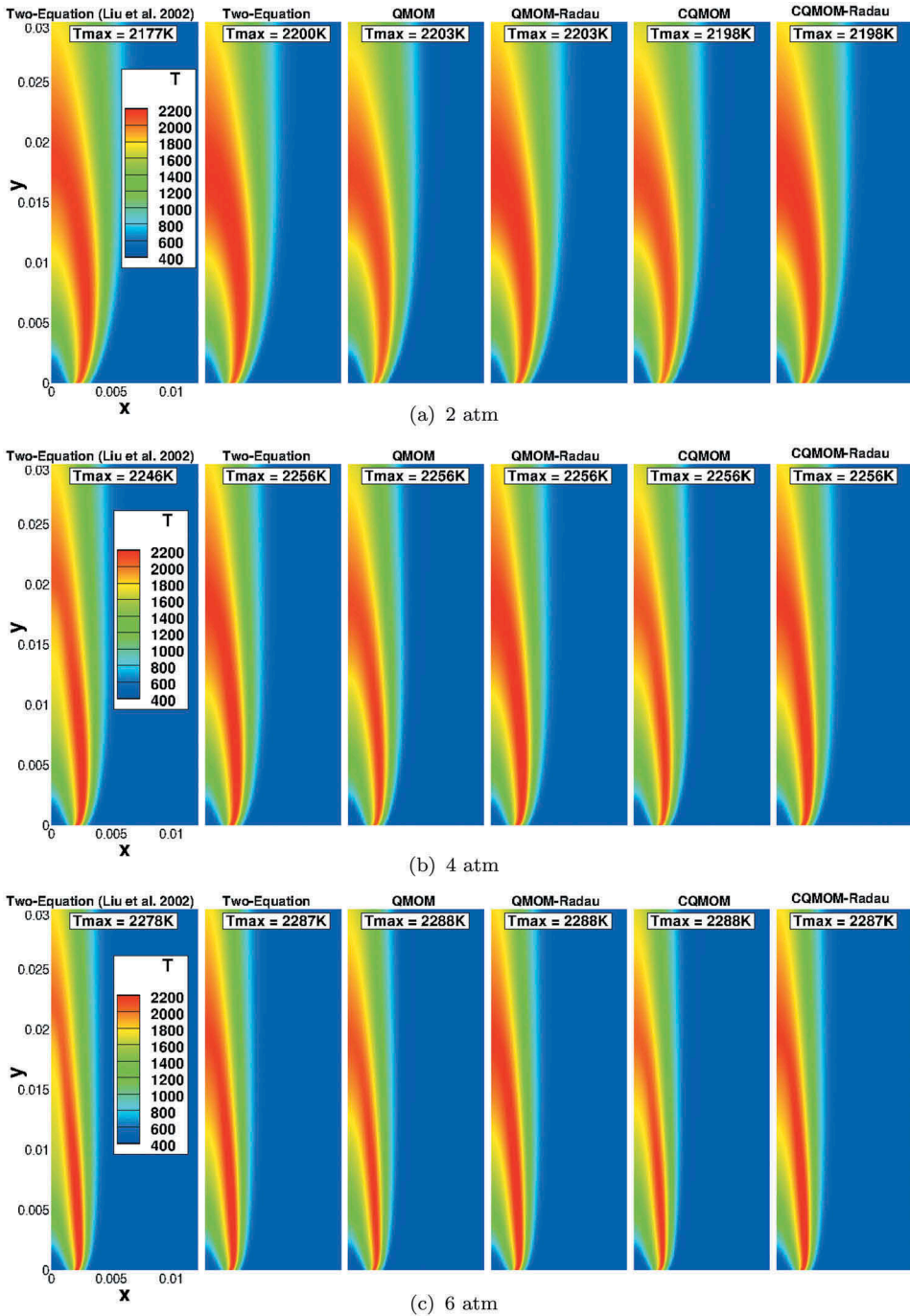


Figure 7. Predicted temperatures distributions for methane/ethanol diffusions flames at (a) 2 atm, (b) 4 atm, and (c) 6 atm.

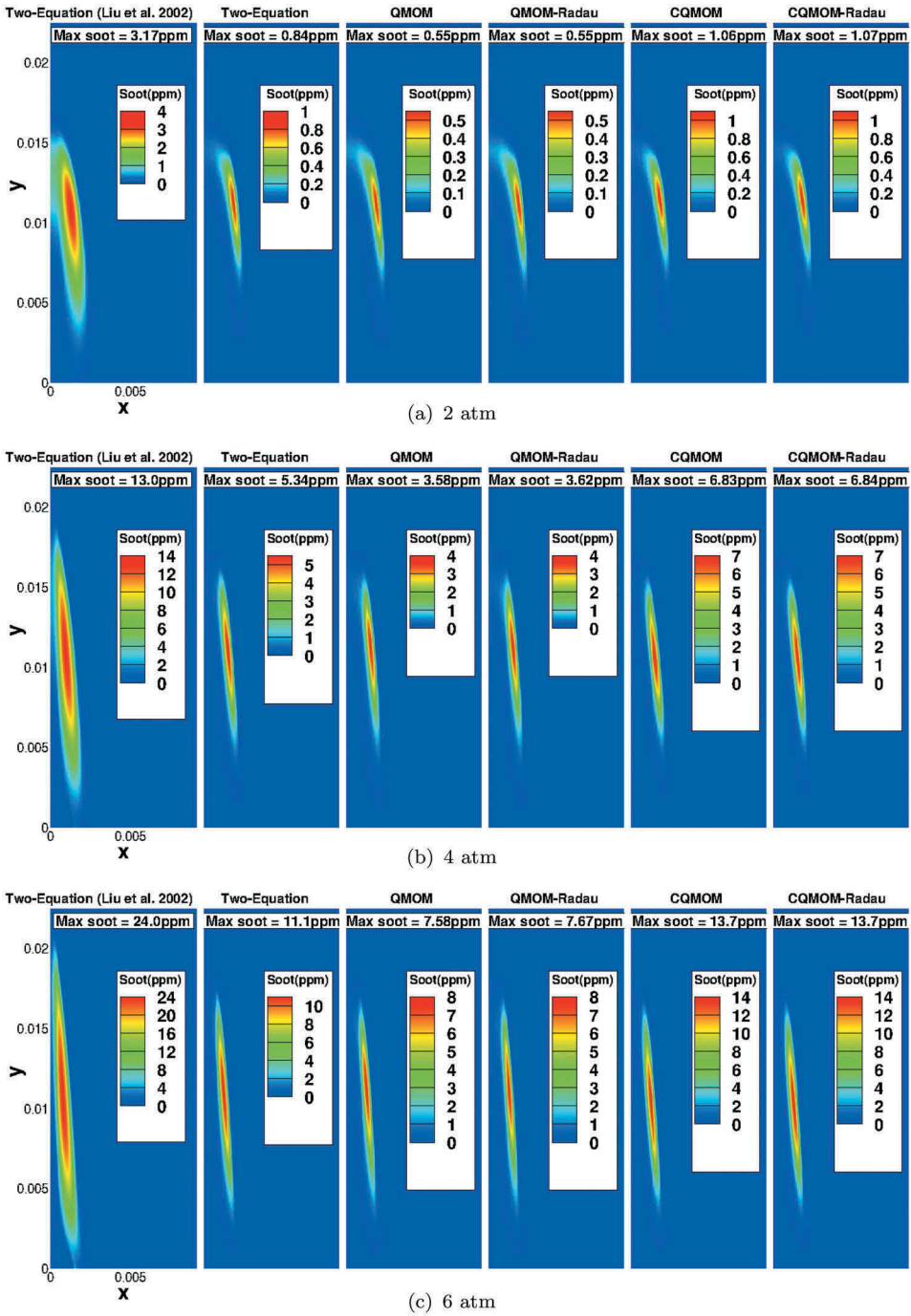


Figure 8. Predicted soot distributions for methane/ethanol diffusion flames at (a) 2 atm, (b) 4 atm, and (c) 6 atm.

Table 5. Experimental and numerical peak soot concentration of elevated pressure methane/ethanol diffusion flames.

	Peak soot concentration (ppm)		
	2 atm	4 atm	6 atm
Experimental	2.1	10.0	21.0
Two-Equation (Liu et al. 2002)	3.17	13.0	24.0
Two-Equation (proposed)	0.84	5.34	11.1
QMOM	0.55	3.58	7.58
QMOM-Radau	0.55	3.62	7.67
CQMOM	1.06	6.83	13.7
CQMOM-Radau	1.07	6.84	13.7

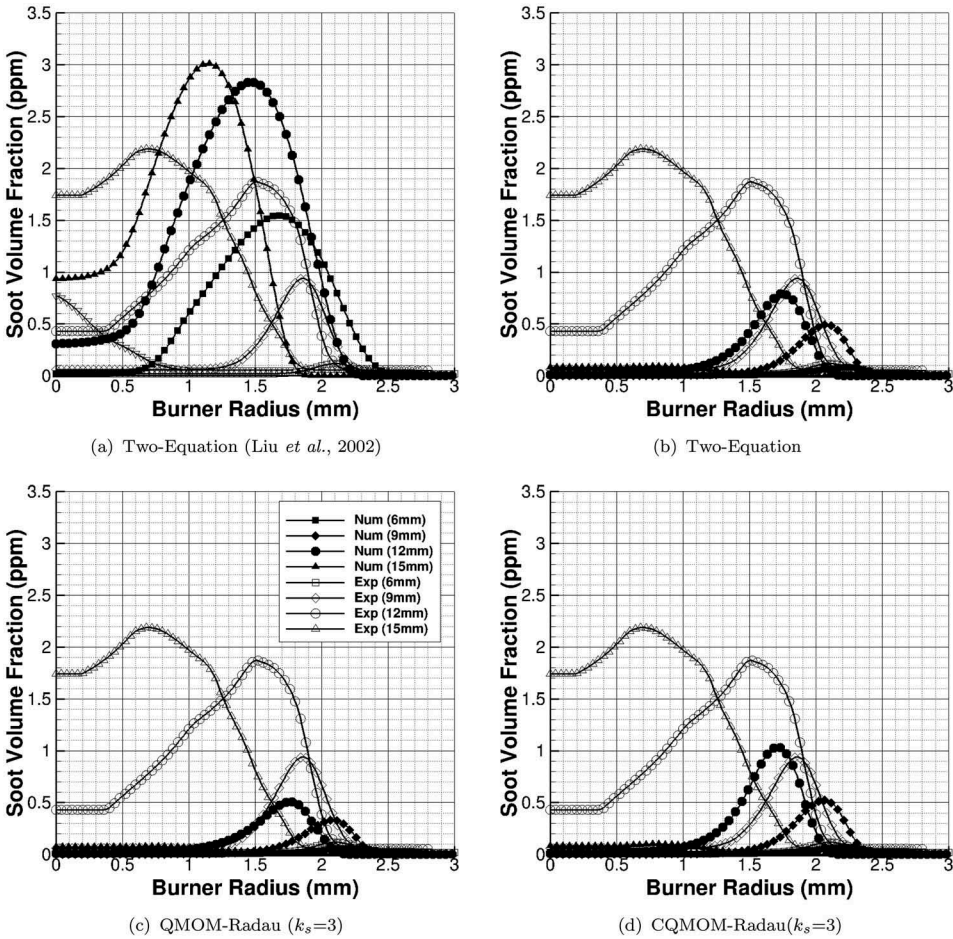


Figure 9. Comparison of numerical and experimental soot volume fraction radial profiles for a coflow methane/ethanol diffusion flame at 2 atm.

Conclusions

The present numerical study has considered the application of quadrature-based moment closure techniques to the prediction of soot formation for a space homogeneous problem

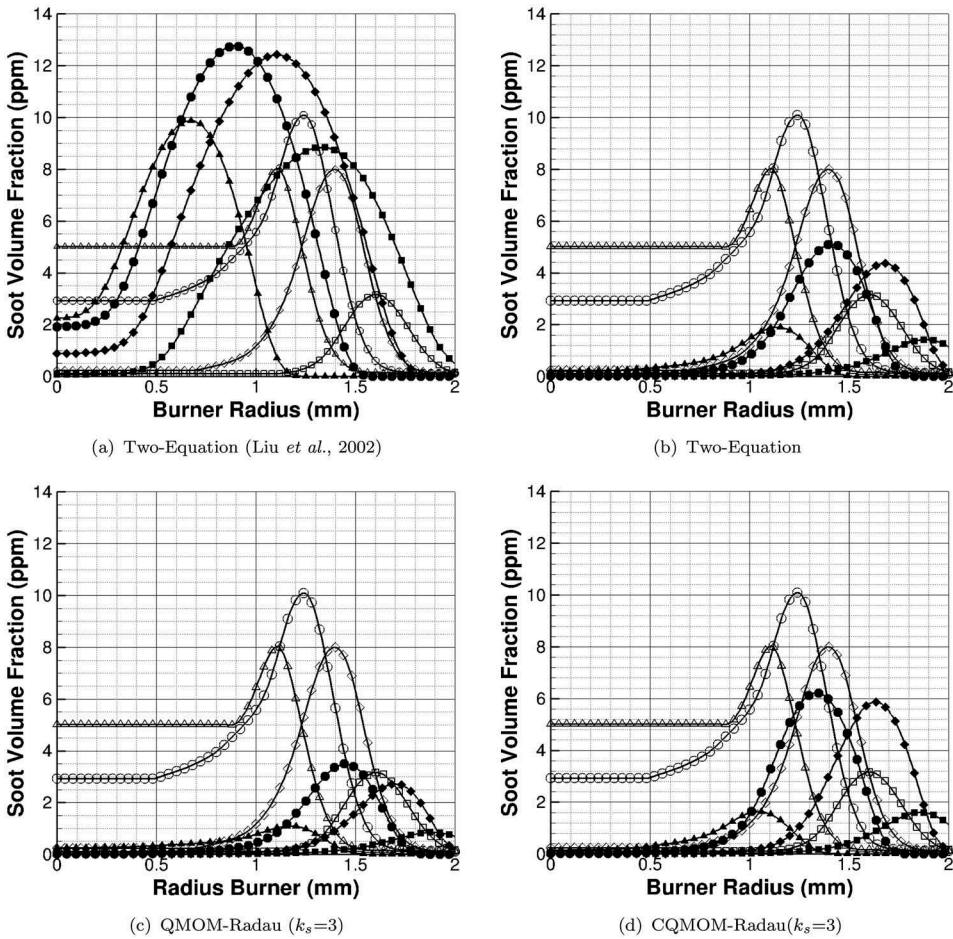


Figure 10. Comparison of numerical and experimental soot volume fraction radial profiles for a coflow methane/ethanol diffusion flame at 4 atm.

and in laminar diffusion flames and shown the importance of using fractional-order moments for the accurate prediction of soot in space-homogeneous problem with a volume-based formulation for soot transport modeling. Notably, the inception mode is not represented appropriately by QMOM approaches when using integer-order moments, unless one quadrature node is explicitly assigned to the inception size as in the QMOM-Radau type closures. This finding is of significant importance as many moment methods make use of integer-order moments (in particular, MOMIC method interpolates unknown moments from integer-order moments). The results for the laminar diffusion flames indicate further that the CQMOM/CQMOM-Radau with $N_V = 3$ and $N_{n_p} = 1$ provide better predictions of peak soot formation than the two-equation model or the QMOM/QMOM-Radau approaches, with equivalent soot chemistry, and may be well suited for the prediction of soot formation in practical engineering devices. However, the predicted centerline soot concentrations were found to be significantly underpredicted because of the non-PAH-based acetylene mechanism applied here. Future research will

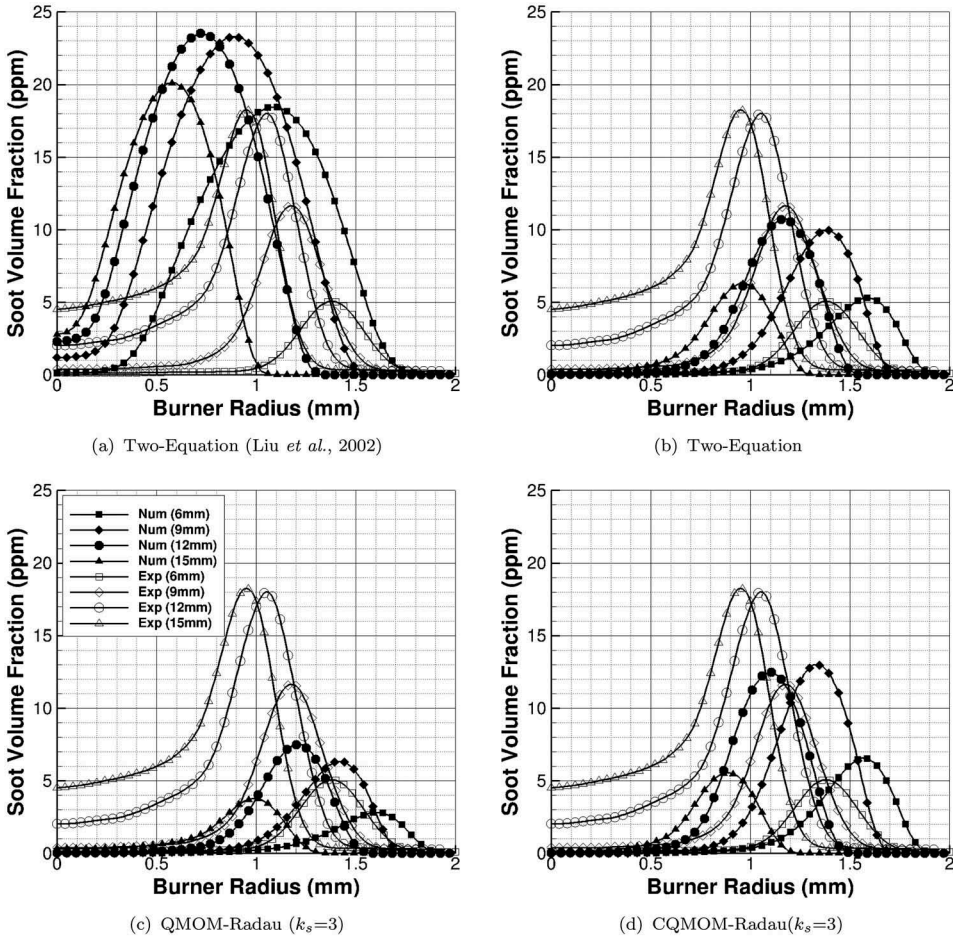


Figure 11. Comparison of numerical and experimental soot volume fraction radial profiles for a coflow methane/ethanol diffusion flame at 6 atm.

consider chemical mechanism containing PAH, PAH-based nucleation, and PAH condensation in order to achieve improved predictions of the centerline soot concentration.

Acknowledgments

This research was funded by grants and contracts from the Green Aviation Research and Development Network (GARDN), Southern Ontario Smart Computing for Innovation Platform (SOSCIP), as well as Pratt & Whitney Canada. The first author also received support in the form of a scholarship from the Natural Sciences and Engineering Research Council (NSERC) of Canada. Additionally, the computational resources for performing the numerical simulations reported herein were provided by the SOSCIP program as well as the SciNet High Performance Computing Consortium at the University of Toronto and Compute/Calcul Canada (the latter are funded by the Canada Foundation for Innovation (CFI) and Province of Ontario, Canada).

References

- Akih-Kumgeh, B. 2013. *Comparison of detailed and reduced models for syngas and ethanol*. Canada: Alternative Fuels Laboratory, Department of Mechanical Engineering, McGill University.
- Appel, J., H. Bockhorn, and M. Frenklach. 2000. Kinetic modeling of soot formation with detailed chemistry and physics: Laminar premixed flames of c2 hydrocarbons. *Combust. Flame* 121 (1–2):122–36. doi:10.1016/S0010-2180(99)00135-2.
- Balthasar, M., and M. Kraft. 2003. A stochastic approach to calculate the particle size distribution function of soot particles in laminar premixed flames. *Combust. Flame* 133:289–98. doi:10.1016/S0010-2180(03)00003-8.
- Bhatt, J. S., and R. P. Lindstedt. 2009. Analysis of the impact of agglomeration and surface chemistry models on soot formation and oxidation. Proceedings of the Combustion Institute, vol. 32, 713–20. McGill University, Canada.
- Blacha, T., M. D. Domenico, P. Gerlinger, and M. Aigner. 2012. Soot predictions in premixed and non- premixed laminar flames using a sectional approach for pahas and soot. *Combust. Flame* 159:181–93. doi:10.1016/j.combustflame.2011.07.006.
- Blanquart, G., and H. Pitsch. 2009. Analyzing the effects of temperature on soot formation with a joint volume-surface-hydrogen model. *Combust. Flame* 156:1614–26. doi:10.1016/j.combustflame.2009.04.010.
- Buffo, A., M. Vanni, and D. L. Marchisio. 2012. Multidimensional population balance model for the simulation of turbulent gas-liquid systems in stirred tank reactors. *Chem. Eng. Sci.* 70:31–44. doi:10.1016/j.ces.2011.04.042.
- Celnik, M., R. Patterson, M. Kraft, and W. Wagner. 2007. Coupling a stochastic soot population balance to gas-phase chemistry using operator splitting. *Combust. Flame* 148:158–76. doi:10.1016/j.combustflame.2006.10.007.
- Chalons, C., R. O. Fox, and M. Massot. 2010. A multi-gaussian quadrature method of moments for gas- particle flows in a les framework. In Proceedings of the summer program 2010, 347–58. Palo Alto, California.
- Charest, M. R., C. P. Groth, and Ö. L. Gülder. 2010. A computational framework for predicting laminar reactive flows with soot formation. *Combust. Theor. Model.* 14:793–825. doi:10.1080/13647830.2010.512960.
- Charest, M. R., C. P. Groth, and Ö. L. Gülder. 2011. Effects of gravity and pressure on laminar coflow methane–Air diffusion flames at pressures from 1 to 60 atmospheres. *Combust. Flame* 158 (5):860–75. doi:10.1016/j.combustflame.2011.01.019.
- Charest, M. R., Ö. L. Gülder, and C. P. Groth. 2014. Numerical and experimental study of soot formation in laminar diffusion flames burning simulated biogas fuels at elevated pressures. *Combust. Flame* 161 (10):2678–91. doi:10.1016/j.combustflame.2014.04.012.
- Charest, M. R., H. I. Joo, Ö. L. Gülder, and C. P. Groth. 2011. Experimental and numerical study of soot formation in laminar ethylene diffusion flames at elevated pressures from 10 to 35 atm. *Proc. Combust. Inst.* 33 (1):549–57. doi:10.1016/j.proci.2010.07.054.
- Clarke, A. D., K. J. Noone, J. Heintzenberg, S. G. Warren, and D. S. Covert. 1967. Aerosol light absorption measurement techniques: Analysis and intercomparisons. *Atmos. Environ.* 21:1455–65. doi:10.1016/0004-6981(67)90093-5.
- D’Anna, A., and J. H. Kent. 2006. Modeling of particulate carbon and species formation in coflowing diffusion flames of ethylene. *Combust. Flame* 144:249–60. doi:10.1016/j.combustflame.2005.07.011.
- Frenklach, M. 2002. Method of moments with interpolative closure. *Chem. Eng. Sci.* 57:2229–39. doi:10.1016/S0009-2509(02)00113-6.
- Frenklach, M., and S. J. Harris. 1987. Aerosol dynamics modeling using the method of moments. *J. Colloid Interface Sci.* 118:252–61. doi:10.1016/0021-9797(87)90454-1.
- Goodson, M., and M. Kraft. 2002. An efficient stochastic algorithm for simulating nano-particle dynamics. *J. Comput. Phys.* 183:210–32. doi:10.1006/jcph.2002.7192.
- Gordon, R. G. 1968. Error bounds in equilibrium statistical mechanics. *J. Math. Phys.* 9:655–63. doi:10.1063/1.1664624.

- Griffin, E. A., M. Christensen, and Ö. L. Gülder. 2018. Effect of ethanol addition on soot formation in laminar methane diffusion flames at pressures above atmospheric. *Combust. Flame* 193:306–12. doi:10.1016/j.combustflame.2018.04.001.
- Kennedy, I. M. 2007. The health effects of combustion-generated aerosols. *Proc. Comb. Inst.* 31:2757–70. doi:10.1016/j.proci.2006.08.116.
- Köylü, Ü. Ö., G. Faeth, T. L. Farias, and M. G. Carvalho. 1995. Fractal and projected structure properties of soot aggregates. *Combust. Flame* 100 (4):621–33. doi:10.1016/0010-2180(94)00147-K.
- Kumar, S., and D. Ramkrishna. 1996. On the solution of population balance equations by discretization i: A fixed pivot technique. *Chem. Eng. Sci.* 51:1311–32. doi:10.1016/0009-2509(96)88489-2.
- Leung, K. M., R. P. Lindstedt, and W. P. Jones. 1991. A simplified reaction mechanism for soot formation in nonpremixed flames. *Combust. Flame* 87:289–305. doi:10.1016/0010-2180(91)90114-Q.
- Liu, F., H. Guo, G. J. Smallwood, and Ö. L. Gülder. 2002. Effects of gas and soot radiation on soot formation in a coflow laminar ethylene diffusion flame. *J. Quant. Spectrosc. Radiat. Transf.* 73:409–21. doi:10.1016/S0022-4073(01)00205-9.
- Madadi-Kandjani, E., and A. Passalacqua. 2015. An extended quadrature-based moment method with log-normal kernel density functions. *Chem. Eng. Sci.* 131:323–39. doi:10.1016/j.ces.2015.04.005.
- Marchisio, D. L., J. T. Piktorna, R. O. Fox, R. D. Vigil, and A. A. Barresi. 2003. Quadrature method of moments for population-balance equations. *AIChE J.* 49:1266–76. doi:10.1002/(ISSN)1547-5905.
- McGraw, R. 1997. Description of aerosol dynamics by the quadrature method of moments. *Aerosol Sci. Technol.* 27:255–65. doi:10.1080/02786829708965471.
- McGraw, R., and D. L. Wright. 2003. Chemically resolved aerosol dynamics for internal mixtures by the quadrature method of moments. *J. Aerosol Sci.* 34:189–209. doi:10.1016/S0021-8502(02)00157-X.
- Menon, S., J. Hansen, L. Nazarenko, and Y. Luo. 2002. Climate effects of black carbon aerosols in china and india. *Science* 297:2255–2253. doi:10.1126/science.1075159.
- Mueller, M. E., G. Blanquart, and H. Pitsch. 2009. Hybrid method of moments for modeling soot formation and growth. *Combust. Flame* 156:1143–55. doi:10.1016/j.combustflame.2009.01.025.
- Patterson, R. I. A., J. Singh, M. Balthasar, M. Kraft, and W. Wagner. 2006. Extending stochastic soot simulation to higher pressures. *Combust. Flame* 145:638–42. doi:10.1016/j.combustflame.2006.02.005.
- Pope, C. A., R. Burnett, M. Thun, E. Calle, D. Krewski, K. Ito, and G. Thurston. 2002. Lung cancer, cardiopulmonary mortality, and long-term exposure to fine particulate air pollution. *JAMA* 287:1132–41. doi:10.1001/jama.287.9.1132.
- Qamar, S., M. Elsner, I. Angelov, G. Warnecke, and A. Seidel-Morgenstern. 2006. A comparative study of high resolution schemes for solving population balances in crystallization. *Chem. Eng. Sci.* 30:1119–31.
- Salenbauch, S., A. Cuoci, A. Frassoldati, C. Saggese, and T. Faravelli. 2015. Modeling soot formation in premixed flames using an extended conditional quadrature method of moments. *Combust. Flame* 162:2529–43. doi:10.1016/j.combustflame.2015.03.002.
- Smooke, M. D., M. B. Long, B. C. Connelly, M. B. Colket, and R. J. Hall. 2005. Soot formation in laminar diffusion flames. *Combust. Flame* 143:613–28. doi:10.1016/j.combustflame.2005.08.028.
- Sung, Y., V. Raman, H. Koo, M. Mehta, and R. O. Fox. 2014. Large eddy simulation modeling of turbulent flame synthesis of titania nanoparticles using a bivariate particle description. *AIChE J.* 60:459–72. doi:10.1002/aic.14279.
- Wheeler, J. C. 1974. Modified moments and gaussian quadratures. *Rocky Mt. J. Math.* 4:287–96. doi:10.1216/RMJ-1974-4-2-287.
- Wick, A., I.-T.-T. Nguyen, F. Laurent, R. O. Fox, and H. Pitsch. 2017. Modeling soot oxidation with the extended quadrature method of moments. *Proc. Comb. Inst.* 36:789–97. doi:10.1016/j.proci.2016.08.004.

- Wright, D. L., R. McGraw, and D. E. Rosner. 2001. Bivariate extension of the quadrature method of moments for modeling simultaneous coagulation and sintering of particle populations. *J. Colloid Interface Sci.* 236:242–51. doi:[10.1006/jcis.2000.7409](https://doi.org/10.1006/jcis.2000.7409).
- Yuan, C., and R. O. Fox. 2011. Conditional quadrature method of moments for kinetic equations. *J. Comput. Phys.* 230:8216–46.
- Yuan, C., F. Laurent, and R. O. Fox. 2012. An extended quadrature method of moments for population balance equations. *J. Aerosol Sci.* 51:1–23. doi:[10.1016/j.jaerosci.2012.04.003](https://doi.org/10.1016/j.jaerosci.2012.04.003).
- Zhang, Q., H. Guo, F. Liu, G. J. Smallwood, and M. J. Thompson. 2008. Implementation of an advanced fixed sectional aerosol dynamics model with soot aggregate formation in a laminar methane/air coflow diffusion flame. *Combust. Theor. Model.* 12:621–41. doi:[10.1080/13647830801966153](https://doi.org/10.1080/13647830801966153).
- Zhao, B., Z. Yang, Z. Li, M. V. Johnston, and H. Wang. 2005. Particle size distribution function of incipient soot in laminar premixed ethylene flames: Effect of flame temperature. Proceedings of the Combustion Institute, vol. 30, 1441–48. University of Illinois at Chicago, United States.
- Zucca, A., D. L. Marchisio, A. A. Barresi, and R. O. Fox. 2006. Implementation of the population balance equation in cfd codes for modelling soot formation in turbulent flames. *Chem. Eng. Sci.* 61:87–95. doi:[10.1016/j.ces.2004.11.061](https://doi.org/10.1016/j.ces.2004.11.061).